MR Spectroscopy for Detecting Fumarate Hydratase Deficiency in Hereditary Leiomyomatosis and Renal Cell Carcinoma Syndrome

Guangyu Wu, MD* • *Guiqin Liu, MD** • *Jianfeng Wang, MD* • *Shihang Pan, BD* • *Yuansheng Luo, BD* • *Yunze Xu, MD* • *Wen Kong, MD* • *Peng Sun, PhD* • *Jianrong Xu, PhD* • *Wei Xue, PhD* • *Jin Zhang, PhD*

From the Departments of Radiology (G.W., G.L., S.P., Y.L., J.X.) and Urology (J.W., Y.X., W.K., W.X., J.Z.), Renji Hospital, School of Medicine, Shanghai Jiao Tong University, Pujian Rd, 200127 Shanghai, China; and Clinical & Technical Solutions, Philips Healthcare, Beijing, China (P.S.). Received November 30, 2021; revision requested February 11, 2022; revision received May 17; accepted June 14. **Address correspondence to** J.Z. (email: *rjzhangjin@126.com*).

* G.W. and G.L. contributed equally to this work.

Conflicts of interest are listed at the end of this article.

Background: Noninvasive in vivo detection of fumarate accumulation may help identify fumarate hydratase deficiency in renal cancer related to hereditary leiomyomatosis and renal cell carcinoma (HLRCC) syndrome.

Purpose: To investigate the feasibility of MR spectroscopy (MRS) in detecting elevated fumarate levels in HLRCC-associated renal cancers.

Materials and Methods: This study included an experimental xenograft mouse model and prospective clinical cohort. First, MRS was performed on patient-derived tumor xenograft models and control models to detect fumarate. Then, consecutive participants with clinical suspicion of HLRCC-associated renal tumors were enrolled. For the detection of fumarate, MRS results were classified as detected, borderline, undetected, or technical failure. The sensitivity, specificity, and accuracy of MRS for diagnosing HLRCC-associated renal cancer were assessed. The signal-to-noise ratio (SNR) of the fumarate peak was calculated and evaluated with receiver operating characteristic curve analysis.

Results: Fumarate peaks were detected at 6.54 parts per million in all three patient-derived xenograft models. A total of 38 participants (21 men; mean age, 47 years [range, 18–71 years]) with 46 lesions were analyzed. All primary HLRCC-associated renal cancers showed a fumarate peak; among the seven metastatic HLRCC-associated lesions, a fumarate peak was detected in three lesions and borderline in two. When only detected peaks were regarded as positive findings, the sensitivity, specificity, and accuracy of MRS at the lesion level were 69% (nine of 13 lesions), 100% (33 of 33 lesions), and 91% (42 of 46 lesions), respectively. When borderline peaks were also included as a positive finding, the sensitivity, specificity, and accuracy reached 85% (11 of 13 lesions), 88% (29 of 33 lesions), and 87% (40 of 46 lesions), respectively. The SNR of fumarate showed an area under the receiver operating characteristic curve of 0.87 for classifying HLRCC-associated tumors.

Conclusion: MR spectroscopy of fumarate was sensitive and specific for hereditary leiomyomatosis and renal cell carcinoma–associated tumors.

© RSNA, 2022

Online supplemental material is available for this article.

Hereditary leiomyomatosis and renal cell carcinoma (HLRCC) is an autosomal-dominant hereditary syndrome caused by germline variations in the fumarate hydratase (FH) gene, which encodes the tricarboxylic acid cycle enzyme FH, resulting in pathologic accumulation of the metabolite fumarate (1–3). The main characteristics of this syndrome are benign smooth-muscle cutaneous uterine tumors (leiomyomas) and an aggressive form of type II papillary renal cell carcinoma (RCC) or collecting duct carcinoma. Although only 15% of individuals with HLRCC develop renal tumors (4), this accounts for the morbidity and mortality burden associated with this syndrome.

According to the National Comprehensive Cancer Network guidelines (NCCN Guidelines for Patients: Kidney Cancer, Version 2.2022) and a previous study (5), prompt surgical extirpation with wide surgical margins and consideration of retroperitoneal lymphadenectomy is recommended without regard to the T stage of HLRCC-associated renal cancer, but radiofrequency ablation, cryotherapy, and active surveillance are not recommended for this patient population. Additionally, treatment regimens for advanced HLRCC-associated renal cancer differ from those for other subtypes (6). Therefore, it is crucial for clinicians to identify individuals at risk (5). Although HLRCC-associated renal cancer has been reported in pathology studies (7,8), diagnosing this disease is still a challenge, even with genetic sequencing (9,10) or histopathologic analysis. Additionally, imaging reports are scarce and lack specificity (11,12) due to disease heterogeneity.

Abbreviations

FH = fumarate hydratase, HLRCC = hereditary leiomyomatosis and renal cell carcinoma, MRS = MR spectroscopy, RCC = renal cell carcinoma, SNR = signal-to-noise ratio

Summary

MR spectroscopy can depict fumarate accumulation in renal cancer related to fumarate hydratase deficiency in hereditary leiomyomatosis and renal cell carcinoma syndrome.

Key Results

- This study consisted of an experimental murine xenograft model and prospective cohort of 38 participants with suspected hereditary leiomyomatosis and renal cell carcinoma (HLRCC)–associated renal cancer; MR spectroscopy was used for fumarate detection.
- Fumarate peaks were detected in HLRCC xenograft models at 6.54 parts per million.
- The sensitivity, specificity, and accuracy of MR spectroscopy for detecting fumarate was 100%, 100%, and 100%, respectively, for the primary tumor and 69%, 100%, and 91% for all lesions.

MR spectroscopy (MRS) is a noninvasive imaging method that can probe steady-state metabolite levels. It has been used as a diagnostic and prognostic tool in patients with cancer and is able to detect the presence of 2-hydroxyglutarate (13), succinate (14), and glycine (15) in vivo in preclinical rodent models and in biopsy samples. Casey et al (16) described the use of MRS to detect fumarate in vivo and successfully detected the peak of fumarate at 6.54 ppm in HLRCC-associated uterine fibroid samples, providing strong evidence for MRS in the evaluation of fumarate levels in patients with HLRCC. However, they were unable to detect a fumarate peak in HLRCC-associated renal tumors (17). Thus, there is a need to further characterize the use of MRS and its ability to detect fumarate in patients with HLRCC-associated renal cancers.

The aim of this study was to investigate the feasibility of MRS in detecting abnormally elevated fumarate levels in HLRCC-associated tumors and to explore the possibility of applying MRS to HLRCC diagnosis.

Materials and Methods

Experimental Evaluation of Fumarate MRS with 7.0-T Animal-dedicated MRI

Patient-derived tumor specimens were collected at Renji Hospital. Animal experiments were approved by the institutional review board (no. 2016-Q22) and the Ethics and Research Committees of Renji Hospital (no. 4–2013–0526). HLRCC-associated patient-derived tumor xenograft and cell-derived xenograft models, SK-RC-39 and Caki-2, respectively, were established for MRS examination. The details of model establishment are provided in Appendix E1 (online). Imaging was performed 39 days ± 12 (SD) on average after grafting. MRS was performed with a dedicated small-animal 7.0-T MRI system (BioSpec 47/40 Ultra Shielded and Refrigerated, Bruker) using a ^{1}H quadrature transmit/receive body coil with a 3.5-cm inner diameter. The MRI protocol is detailed in Appendix E2 (online).

Clinical Evaluation of Fumarate MRS

Participants.—For the prospective case series, participants were recruited from a dedicated urology tumor clinic at Renji Hospital, and all the participants provided written informed consent. The study was approved by the Ethics and Research Committees of Renji Hospital (institutional ethics approval no. KY2018–212). Between August 2019 and March 2022, consecutive participants with a clinical suspicion of HLRCC-associated renal cancer were eligible for inclusion. According to a previous study (18), for inclusion, participants should have a primary renal tumor and meet at least one of the following conditions: *(a)* a family history of FH variation; *(b)* multiple cutaneous leiomyomas, particularly with characteristic shooting pain; *(c)* one or more piloleiomyomas with characteristic shooting pain; and *(d)* in women, the onset of severely symptomatic uterine leiomyomas before 40 years of age.

Historically, HLRCC has been poorly understood, which has led to misdiagnosis, especially in patients with type II papillary RCC. Considering that treatment for HLRCC differs from that for other RCCs, we also enrolled participants with recurrent type II papillary RCC. The exclusion criteria were as follows: *(a)* a lack of MRS examination data; *(b)* solid portions of the tumor less than 1.0 cm; and *(c)* incomplete histopathologic results. Details are shown in Figure 1.
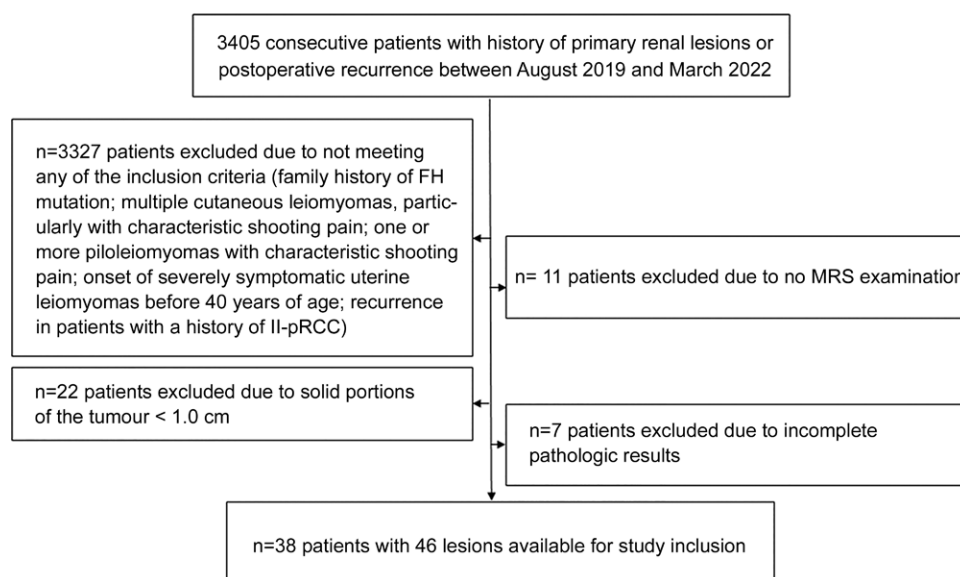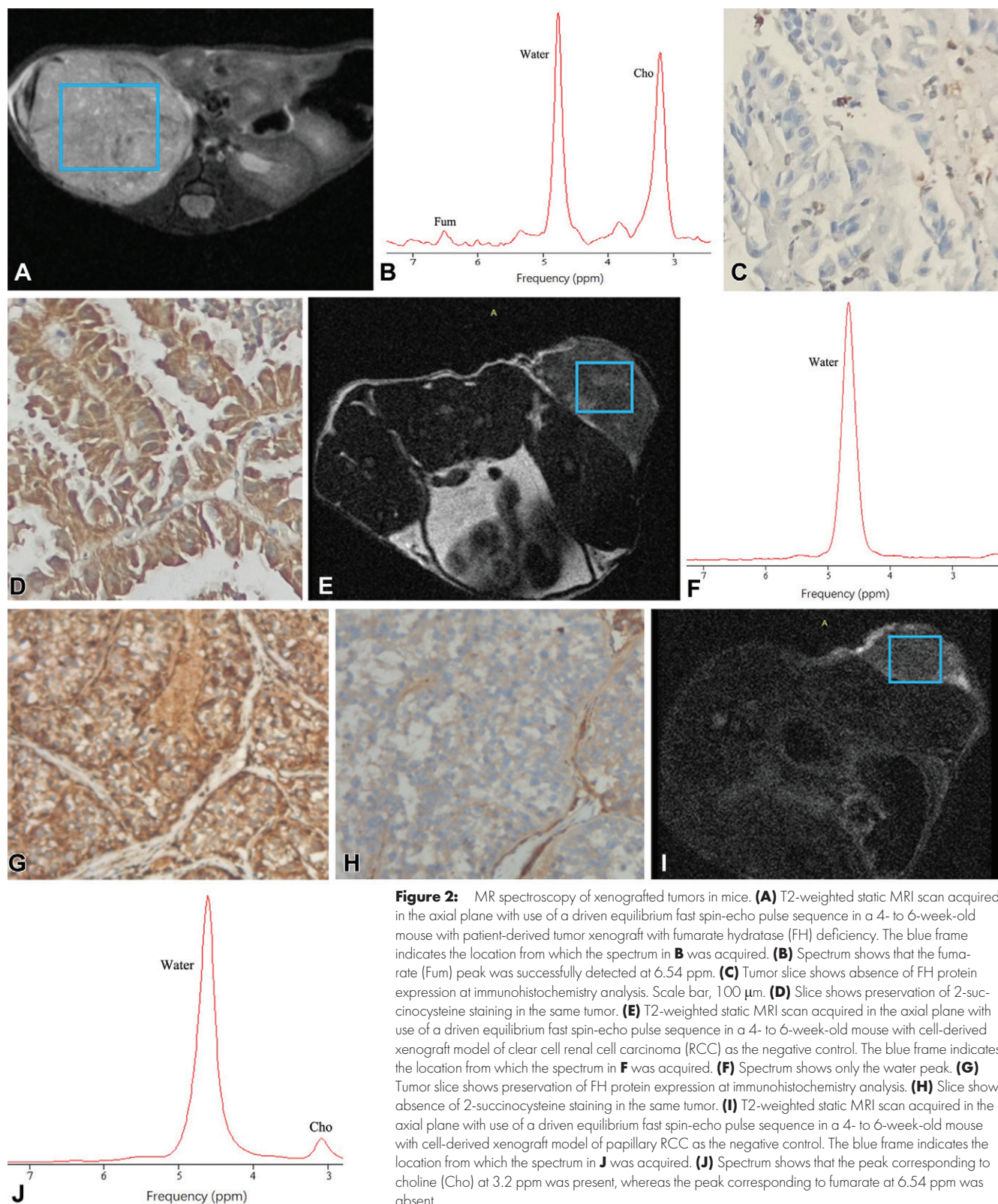

Figure 1: Flowchart for the selection of the participant sample in the current study. II-pRCC = type II papillary renal cell carcinoma, FH = fumarate hydratase, MRS = MR spectroscopy.

Figure 2: MR spectroscopy of xenografted tumors in mice. **(A)** T2-weighted static MRI scan acquired in the axial plane with use of a driven equilibrium fast spin-echo pulse sequence in a 4- to 6-week-old mouse with patient-derived tumor xenograft with fumarate hydratase (FH) deficiency. The blue frame indicates the location from which the spectrum in **B** was acquired. **(B)** Spectrum shows that the fumarate (Fum) peak was successfully detected at 6.54 ppm. **(C)** Tumor slice shows absence of FH protein expression at immunohistochemistry analysis. Scale bar, 100 μm. **(D)** Slice shows preservation of 2-succinocysteine staining in the same tumor. **(E)** T2-weighted static MRI scan acquired in the axial plane with use of a driven equilibrium fast spin-echo pulse sequence in a 4- to 6-week-old mouse with cell-derived xenograft model of clear cell renal cell carcinoma (RCC) as the negative control. The blue frame indicates the location from which the spectrum in **F** was acquired. **(F)** Spectrum shows only the water peak. **(G)** Tumor slice shows preservation of FH protein expression at immunohistochemistry analysis. **(H)** Slice shows absence of 2-succinocysteine staining in the same tumor. **(I)** T2-weighted static MRI scan acquired in the axial plane with use of a driven equilibrium fast spin-echo pulse sequence in a 4- to 6-week-old mouse with cell-derived xenograft model of papillary RCC as the negative control. The blue frame indicates the location from which the spectrum in **J** was acquired. **(J)** Spectrum shows that the peak corresponding to choline (Cho) at 3.2 ppm was present, whereas the peak corresponding to fumarate at 6.54 ppm was absent.

MRS with 3.0-T MRI

Clinical MRS studies were performed with a 3.0-T MRI system (Magnetom Prisma, Siemens Healthineers) with body coil transmission and 18-channel receiver coils. A minimum solid portion of the tumor size threshold of 1.0 cm was applied for inclusion in the study; on this basis, the largest lesion was selected as the target for primary and/or metastatic lesions.

The MRI protocol included T2-weighted fast spin-echo and Dixon T1 gradient-echo sequences with dynamic contrast enhancement. MRS was carried out using a point-resolved

Table 1: Characteristics of the 11 Participants with HLRCC-associated Renal Tumors Analyzed with MRS at 3.0 T

Participant No.	Sex	Age (y)	Variation Type	Primary Tumor	Metastatic Disease	Site of MRS	Tumor Diameter (mm)	VOI Size (cm³)	Fumarate Peak	Complicated with Uterine/ Cutaneous Lesions	History of Treatment before MRS
1	M	54	c.237dupT (p.K80X)	Yes	No	Kidney	61	23.4	Detected	No	Sunitinib
2	M	33	c.294 delC	No	Yes	Lymph node	32	4.6	Undetected	Yes	Pembrolizumab + lenvatinib
3	M	38	C.698G>A	Yes	No	Kidney	113	20.3	Detected	No	Bevacizumab + erlotinib
3	…	…	…	No	Yes	Retroperitoneum	42	6	Borderline	NA	NA
4	M	68	het del in exon 1	No	Yes	Bone	2.9	1.6	Technical failure	No	NA
5	F	39	het del in exon 1–10	Yes	No	Kidney	114	26.1	Detected	Yes	NA
5	…	…	…	No	Yes	Lymph node	34	2.4	Detected	NA	NA
6	M	65	c.717_718insAGCA	No	Yes	Pelvic cavity	86	25.2	Detected	No	NA
7	M	38	het del variation in exon 9	No	Yes	Liver	62	6.5	Borderline	No	Lenvatinib + nivolumab
8	F	23	het del variation c 1–10	Yes	No	Kidney	37	5.4	Detected	Yes	NA
9	M	71	c.823G>A	Yes	No	Kidney	109	27	Detected	No	NA
10	F	29	p.k223fs*26	No	Yes	Retroperitoneum	65	27	Detected	Yes	NA
11	M	48	c.1268TG	Yes	No	Kidney	43	5.8	Detected	No	NA

Note.—del = deletion, het = heterozygous, HLRCC = hereditary leiomyomatosis and renal cell carcinoma, MRS = MR spectroscopy, NA = not applicable, VOI = volume of interest.

spectroscopy monovoxel acquisition with a presaturation band placed around the volume of interest (Appendix E3 [online] provides details on sequence parameters). The MRS spectrum of fumarate ($C_4H_2O_4^{-2}$) presents a characteristic peak at 6.54 ppm, with a range from 6.44–6.64 ppm. The volume of interest (1.3–27.0 cm³) was centered on the anatomic image to prevent lipid contamination from the surrounding tissue, as previously described (19).

MRS Analysis
MRS examinations were analyzed with jMRUI software (version 6.0; MRUI Consortium). The signal-to-noise ratio (SNR) was evaluated semiquantitatively in accordance with a previous study (20). Because it was assumed that choline should be detectable in a metabolically active tumor, an MRS examination was regarded as a technical failure if choline was not detected. An expert spectroscopist (G.W., with 10 years of experience in MRS imaging) rated whether the choline peaks were detected (SNR ≥2.0). Three independent investigators (G.L., S.P., and G.W., with 9, 4, and 10 years of experience, respectively, in MRS imaging) who were blinded to the clinical observations and genetic test results at the time of analysis examined all spectra in a qualitative manner and scored the fumarate peak at 6.54 ppm as detected, undetected, or borderline; borderline was defined as an ambiguous peak at 6.54 ppm that was difficult for the investigator to clearly classify as a positive or negative result. When spectral interpretation differed among the three investigators, the principle of majority rule was adopted. When the three interpretations were each different, the discordance was resolved by consultation with another senior physician (J.X., with 30 years of experience in MRS imaging). In cases of technical failure, the SNR of fumarate was assigned a value of 0.

Genotyping and Immunohistochemistry
Germline and somatic FH variations were identified with use of matched tumor-normal next-generation sequencing using Sanger sequencing and multiplex ligation-dependent probe amplification. Tumor slices fixed in formalin and embedded in paraffin were used for FH and 2-succinocysteine staining. Immunohistochemistry analysis was carried out using the EnVision kit (Dako) according to the manufacturer's protocol.

Statistical Analysis
Statistical analyses were performed using SPSS 19.0 (IBM). Continuous variables are expressed as means ± SDs, and categorical variables are expressed as frequencies with percentages. A diagnostic test should correctly identify disease and nondisease states to determine the true accuracy, which involves several important indicators: sensitivity, specificity, and accuracy. These three indicators were adopted to evaluate the diagnostic performance of MRS for HLRCC. Interobserver agreement and the robustness of the MRS results were assessed using the Kendall coefficient of concordance (W). The results were interpreted according to Martin and Bateson (21), where $W = 0.0$–0.2 indicates a slight correlation, $W = 0.21$–0.4 indicates a low correlation, $W = 0.41$–0.7 indicates a moderate correlation, $W = 0.71$–0.9 indicates a high correlation, and $W = 0.91$–
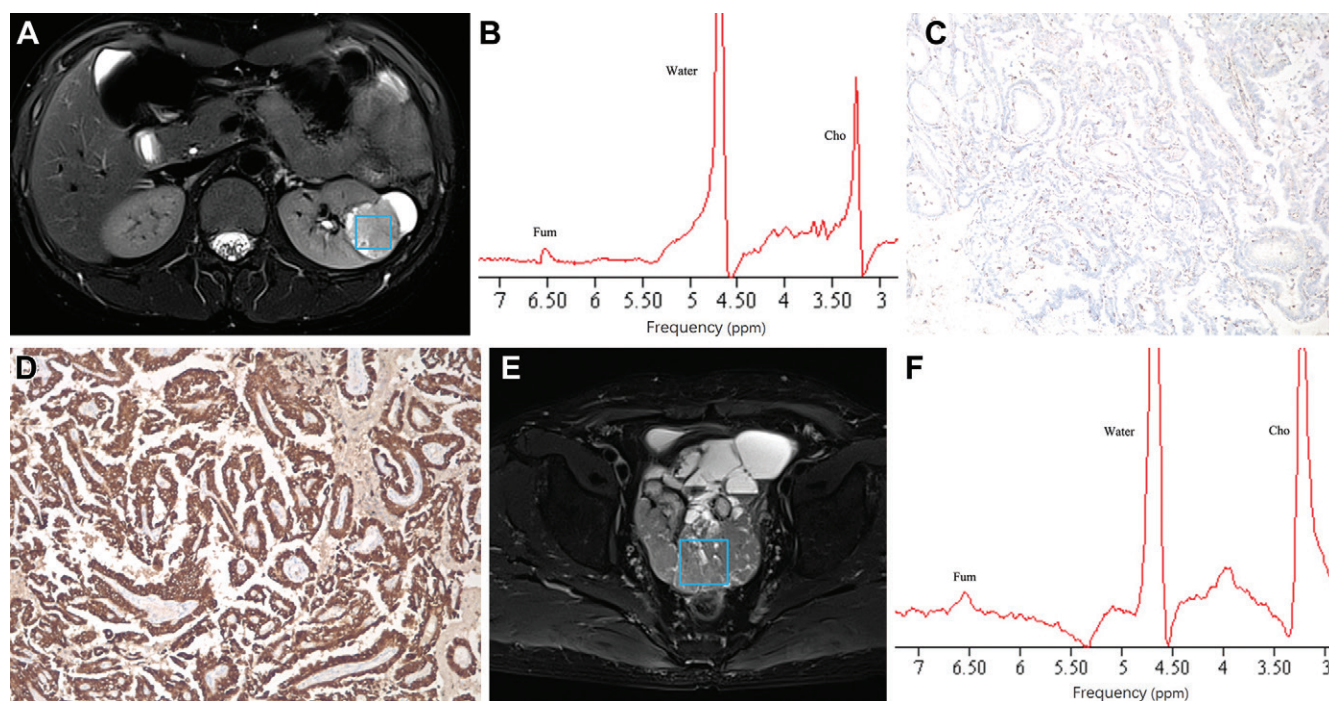
Figure 3: Representative cases of a primary renal tumor and metastatic lesion with fumarate hydratase deficiency. **(A)** Axial T2-weighted static image acquired using a fast spin-echo pulse sequence in a 23-year-old woman (patient 8 in Table 1) with hematuria. A myomectomy was performed 3 years before the image acquisition date. The blue frame indicates the location from which the spectrum in **B** was acquired. **(B)** Spectrum demonstrates a fumarate (Fum) peak detected at 6.54 ppm. **(C)** Slice shows the loss of fumarate hydratase protein expression, which was confirmed after radical nephrectomy. Scale bar, 200 μm. **(D)** Slice shows preserved 2-succinocysteine staining in the same tumor. **(E)** Axial T2-weighted static image acquired using a fast spin-echo pulse sequence in a 65-year-old man (patient 6 in Table 1) with pelvic cavity metastasis. A radical nephrectomy was performed 3 months before the image acquisition date. The blue frame indicates the location from which the spectrum in **F** was acquired. **(F)** Spectrum shows that fumarate peaks were successfully detected at 6.54 ppm. Cho = choline.
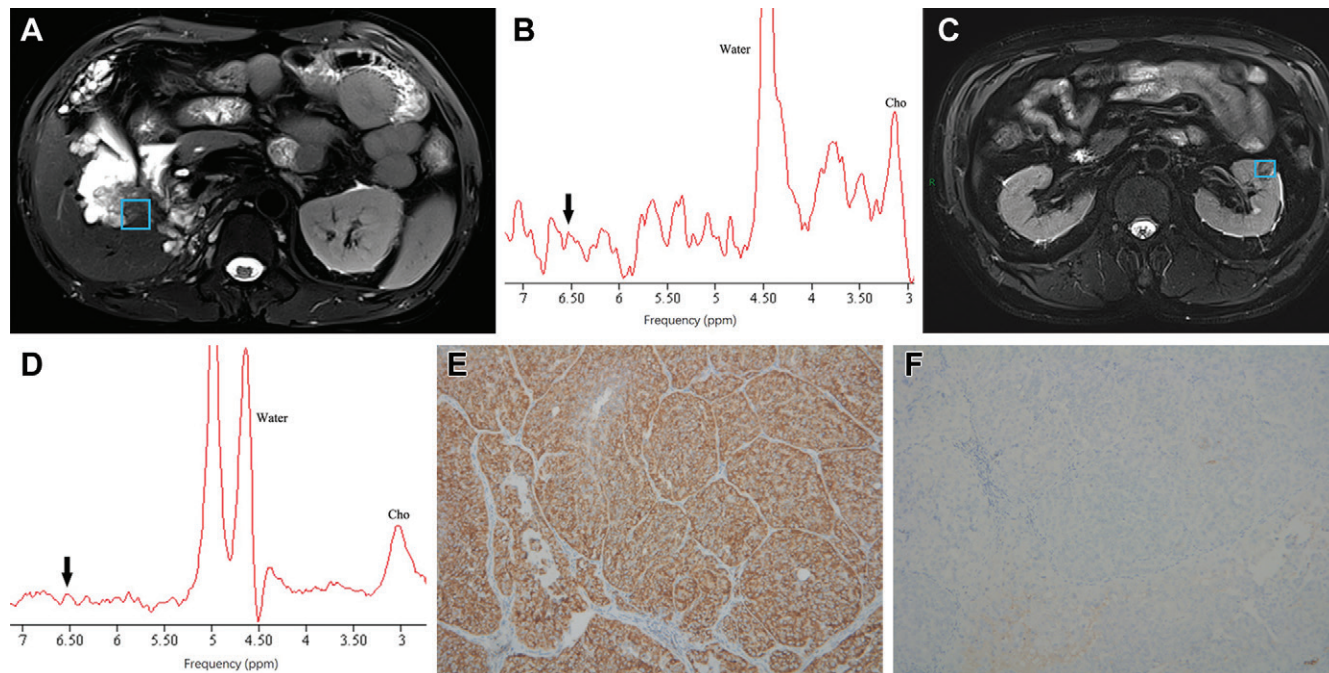

Figure 4: Representative MR spectroscopy images with borderline fumarate peaks. **(A)** Axial T2-weighted static image acquired using a fast spin-echo pulse sequence in a 38-year-old man (patient 7 in Table 1) with a germline heterozygous deletion allelic variation demonstrates liver metastasis. A radical nephrectomy was performed 1 year before the image acquisition date. The blue frame indicates the location from which the spectrum in **B** was acquired. **(B)** Spectrum processed with jMRUI shows a broad, unconvincing, and unreliable peak (arrow) at 6.54 ppm. **(C)** Axial T2-weighted static image acquired using a fast spin-echo pulse sequence in a 68-year-old man (patient 17 in Table E2 [online]) with a primary left renal mass pathologically confirmed as type II papillary renal cell carcinoma. The blue frame indicates the location from which the spectrum in **D** was acquired. **(D)** Spectrum shows that a choline (Cho) peak at 3.2 ppm was successfully detected, and an unreliable peak (arrow) at 6.54 ppm was observed. **(E)** Immunohistochemically stained tumor slice reveals the preservation of fumarate hydratase protein expression in the left renal mass. Scale bar, 200 μm. **(F)** Slice shows absence of 2-succinocysteine staining in the same tumor.
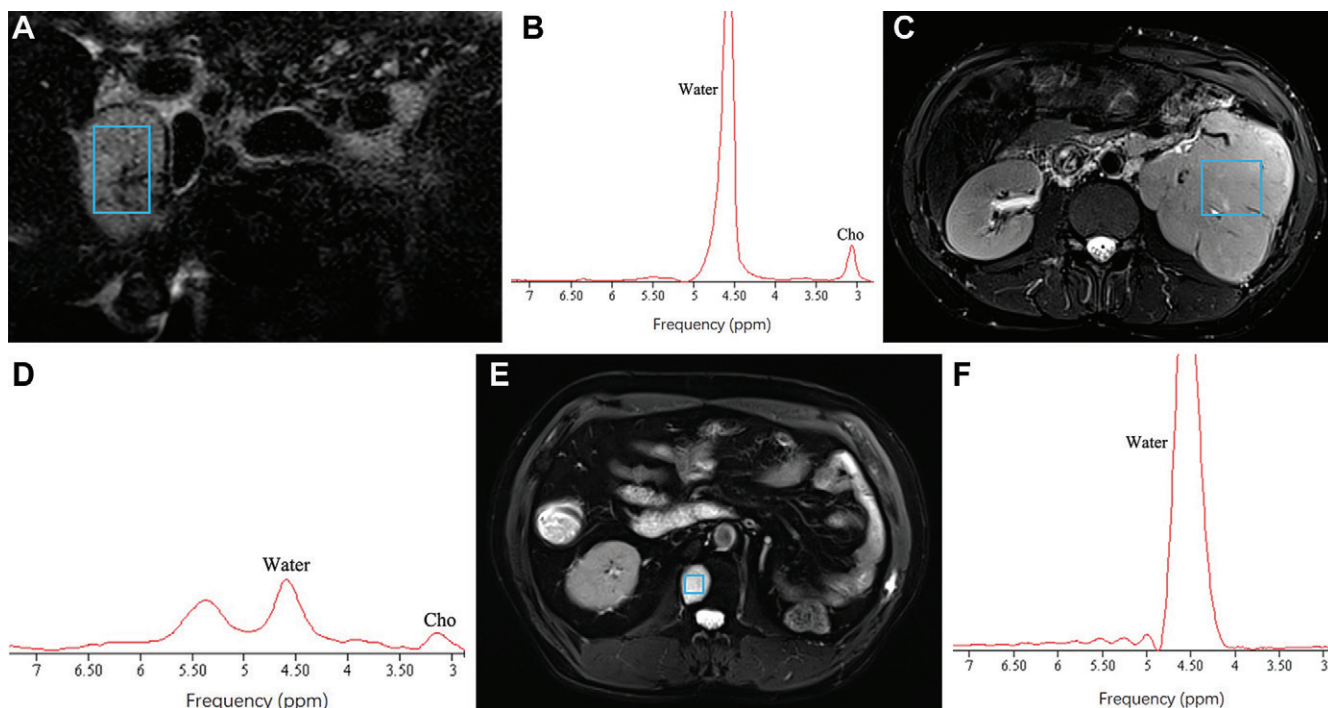
Figure 5: Representative cases of undetected fumarate peaks and technical failure. **(A)** Axial T2-weighted static images acquired using a fast spin-echo pulse sequence in a 33-year-old man (patient 2 in Table 1) with fumarate hydratase deficiency–associated lymph node metastasis. A radical nephrectomy was performed 9 months before the image acquisition date. The blue frame indicates the location from which the spectrum in **B** was acquired. **(B)** Spectrum shows that the choline (Cho) peak at 3.2 ppm was successfully detected, whereas the fumarate peak at 6.54 ppm was absent. **(C)** Axial T2-weighted static image acquired using a fast spin-echo pulse sequence in a 51-year-old woman (patient 13 in Table E2 [online]) with a primary left renal mass pathologically confirmed as spindle cell sarcoma. The blue frame indicates the location from which the spectrum in **D** was acquired. **(D)** Spectrum shows that the fumarate peak at 6.54 ppm was absent, but the choline peak was present. **(E)** Axial T2-weighted static image acquired using a fast spin-echo pulse sequence in a 68-year-old man (patient 4 in Table 1) with hereditary leiomyomatosis and renal cell carcinoma–associated lumbar spine metastasis. A radical nephrectomy was performed 2 years before the image acquisition date. The blue frame indicates the location from which the spectrum in **F** was acquired. **(F)** Spectrum shows the absence of fumarate and choline.

1.0 indicates a very high correlation. The performance of the SNR was evaluated with receiver operating characteristic curve analysis and the area under the receiver operating characteristic curve. *P* < .05 was considered indicative of statistically significant difference.

Results

In Vivo Detection of Fumarate in Murine Xenograft Tumors

In the preclinical study, patient-derived tumor xenograft models of HLRCC-associated RCC (Fig 2A–2D) as well as cell-derived xenograft models of clear cell RCC and papillary RCC (Fig 2E–2J) were generated. FH and 2-succinocysteine were measured to confirm the inhibition of FH activity in HLRCC-associated RCC. MRS examinations were evaluated in mice, with an echo time of 140 msec and a fixed volume-of-interest size (125–250 mm³) placed over the tumor mass in each model. The peak corresponding to choline was consistently present in the HLRCC-associated (Fig 2B) and papillary RCC (Fig 2J) tumors, while the clear cell RCC tumors showed only a water peak (Fig 2F). Moreover, the fumarate peak was detected only in HLRCC-associated renal tumors (Fig 2B), and the SNR of fumarate ranged from 5.81–19.35 for HLRCC-associated RCC and from 0.85–1.22 for papillary RCC and clear cell RCC.

Participant Characteristics

Among the 3405 consecutive participants originally eligible for inclusion, 3367 were excluded, leaving 38 participants (mean age, 47 years [range, 18–71 years]; 21 men and 17 women) with 46 lesions for analysis. Lesion characteristics of imaging presentations are summarized in Tables 1 and E1 (online). A total of 11 participants (median age, 46 years [range, 23–71 years]; eight men and three women) with 13 lesions were diagnosed with HLRCC-associated RCC or related metastatic lesions based on the FH germline variations and immunohistochemistry results of tumor tissue showing absent FH immunostaining. Among these participants, four had only primary renal tumors, two presented with primary renal tumors and metastasis, and five developed metastatic lesions following partial or radical nephrectomy. Demographic and clinical characteristics are shown in Table 1. The demographic and clinical characteristics of the remaining 27 participants with 33 lesions are summarized in Table E2 (online).

Repeatability in MRS Analysis of Fumarate

The repeatability of the MRS results was evaluated twice in the same tumor for 14 participants during the same examination (four participants from the HLRCC-associated RCC group and 10 from the negative control group). The results for fumarate were
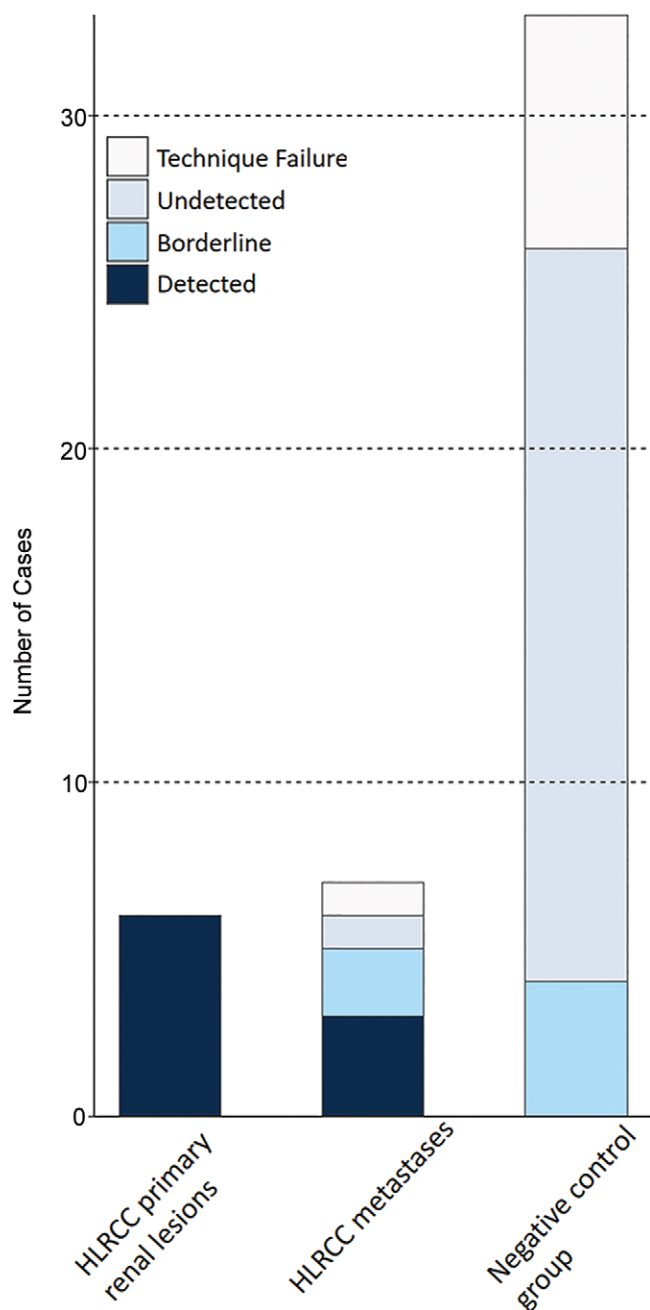
Figure 6: Component bar graph shows the MR spectroscopy results of hereditary leiomyomatosis and renal cell carcinoma (HLRCC)–associated primary lesions and metastases and the negative control group.

almost identical in these participants (W = 0.98; P = .02), suggesting very high test reproducibility (Table E3 [online]). For the 38 lesions with successful spectral imaging, the W coefficient among the interpretations of the three investigators was 0.96 (P < .001), demonstrating excellent agreement. There were no evaluations in which the three interpretations were each different, so the final diagnoses were made without the intervention of a more senior radiologist.

MRS Fumarate Peak Detected in Participants with HLRCC
Fumarate was detected at 6.54 ppm in nine lesions from eight participants, all of whom were confirmed to have HLRCC,

including six primary renal tumors and three metastatic lesions (see Figure 3 for representative cases); moreover, no fumarate peak was detected in lesions without FH deficiency.

Borderline Fumarate Peaks Detected
Borderline fumarate peaks were detected in six participants with six lesions, including two primary renal tumors and four metastatic lesions; two lesions were FH-deficient, and four lesions did not have FH deficiency (see Fig 4 for representative cases).

Fumarate Peak Undetected and Technical Failure
The fumarate peak was not detected in 19 participants with 23 lesions, including 13 primary renal tumors and 10 metastatic lesions, of which only one metastatic lesion was confirmed to be HLRCC. Technical failure occurred in eight participants with eight lesions, including five primary renal tumors and three metastatic lesions, of which only one lesion was associated with HLRCC and seven lesions with preserved FH expression (see Fig 5 for representative cases).

Diagnostic Performance
Finally, all the FH-deficient primary renal lesions (six of six) had a fumarate peak. Among the seven metastatic FH-deficient lesions, three were classified as detected and two as borderline. There was only one undetected lesion and one lesion with technical failure in the metastatic group. In the negative control group, in which the lesions proved to have preserved FH expression, no primary renal lesions or metastases had a detected fumarate peak (0 of 33). Of the 20 primary renal lesions, 13 were undetected, two were borderline, and five were technical failure. Of the 13 metastatic lesions, nine were undetected, two were borderline, and two were technical failure. The MRS results of the HLRCC primary lesions, metastases, and negative control group are presented in Figure 6.

When the primary and metastatic lesions were evaluated separately, the accuracy for detected or detected combined with borderline results was 100% (26 of 26) and 92% (24 of 26), respectively, for primary lesions and 80% (16 of 20) and 80% (16 of 20) for metastases. In terms of the diagnostic performance, when the detection of the fumarate peak (ie, detected) was considered a positive result and borderline, undetected, and technical failure were considered a negative result, the sensitivity, specificity, and accuracy of MRS for both primary tumors and metastases were 69% (nine of 13 lesions), 100% (33 of 33 lesions), and 91% (42 of 46 lesions), respectively. If borderline lesions were classified as a positive result, the sensitivity, specificity, and accuracy were 85% (11 of 13 lesions), 88% (29 of 33 lesions), and 87% (40 of 46 lesions), respectively. Details are shown in Table 2. Finally, the diagnostic performance of the SNR of fumarate was evaluated for differentiating lesions with and without FH deficiency. The area under the receiver operating characteristic curve was 0.87 (95% CI: 0.74, 0.95) (Fig 7).

Discussion
In this study, we investigated the feasibility of MR spectroscopy (MRS) in detecting abnormally elevated fumarate levels with use

Table 2: Diagnostic Performance of MR Spectroscopy for Participants

Detection and Lesion Type	Accuracy	Sensitivity	Specificity
Detected as a positive result*			
All lesions	42/46 (91 [78, 97])	9/13 (69 [39, 90])	33/33 (100 [87, 100])
Primary lesions	26/26 (100 [84, 100])	6/6 (100 [52, 100])	20/20 (100 [80, 100])
Metastases	16/20 (80 [56, 93])	3/7 (43% [12, 80])	13/13 (100 [72, 100])
Detected combined with borderline as a positive result†			
All lesions	40/46 (87 [73, 95])	11/13 (85 [54, 97])	29/33 (88 [71, 96])
Primary lesions	24/26 (92 [73, 99])	6/6 (100 [52, 100])	18/20 (90 [67, 98])
Metastases	16/20 (80 [56, 93])	5/7 (71 [30, 95])	11/13 (85 [54, 97])

Note.—Data are numbers of lesions, with percentages in parentheses and 95% CIs in brackets.

* The detection of the fumarate peak is regarded as a positive result, and the remainder (borderline, undetected, and technical failure) is regarded as a negative result.

† Detection and borderline detection are regarded as a positive result, and the remainder (undetected and technical failure) is regarded as a negative result.
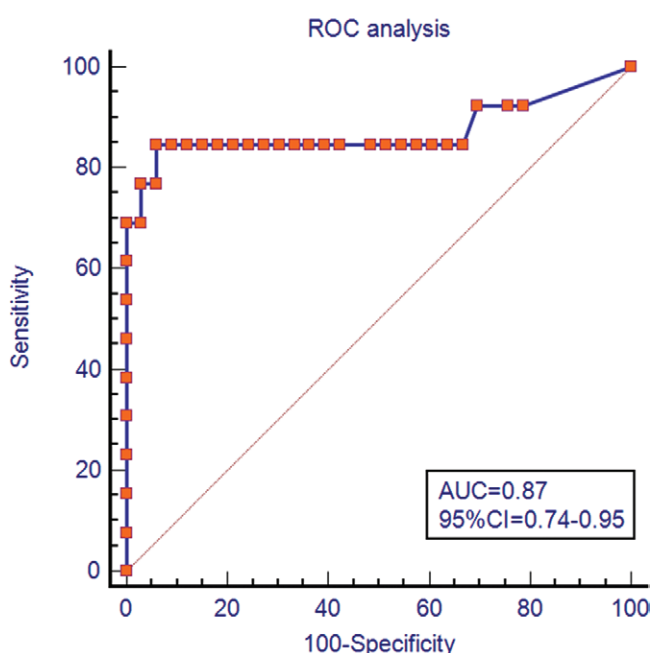

Figure 7: Receiver operating characteristic (ROC) curve analysis of the diagnostic performance of the signal-to-noise ratio of the fumarate peak in differentiating tumors with and without fumarate hydratase deficiency. The orange line represents the reference line. AUC = area under the receiver operating characteristic curve.

of an experimental xenograft mouse model and prospective clinical research. All three of the models of xenografts derived from patients with hereditary leiomyomatosis and renal cell carcinoma (HLRCC) syndrome showed a detectable fumarate peak not present in the control-animal group. In clinical research, all six primary HLRCC-associated renal lesions had a fumarate peak. The sensitivity, specificity, and accuracy of MRS were 69%, 100%, and 91%, respectively, for diagnosing HLRCC-associated renal cancer.

It remains challenging to accurately diagnose HLRCC-associated renal cancer. Even at the pathologic level, current available FH antibodies result in a certain proportion of false-negative or false-positive results. Additionally, the 2-succinocysteine antibody is not yet commercialized and has not been widely adopted

(22–25). Thus, not all pathology departments can accurately diagnose HLRCC-associated renal cancer. The radiologic appearance of renal tumors in patients with HLRCC is highly variable (11,26–29). Improving diagnosis with MRS would be of clinical importance. Many hospitals are equipped with MRI scanners, and MRS scanning capabilities are available on most scanners. Many potential misdiagnoses of HLRCC-associated RCC might be avoided with the application of MRS. It is not only important for the patients themselves but also their family members, who may also have the same allelic variations. Accurate diagnosis may enable their relatives with FH deficiency to be diagnosed earlier and have a better prognosis.

In a previous study, Casey et al (16) attempted to apply MRS to renal lesions to gain further metabolic evidence in support of the pathogenicity of the identified FH variant but were unsuccessful. Unlike uterine fibroid imaging, MRS may be more difficult to perform successfully for primary or metastatic HLRCC-associated RCC, as these lesions may have smaller diameters, limiting the volume available for MRS and leading to a decrease in the quality of MRS (30). However, the results for a single case may exhibit a large bias. In our study, all primary FH-deficient lesions were assessed, and a fumarate peak was detectable. However, considering the several metastatic lesions that were borderline, undetected, or a technical failure, further research is needed to explore contributory factors.

The successful identification of the accumulation of fumarate in HLRCC-associated RCC might have value in a wide range of clinical scenarios, including assessing patients with germline FH variants of uncertain clinical importance and who potentially have FH-deficient tumors, evaluating patients with multiple primary tumors to determine whether any or all are FH-deficient, identifying patients without detectable germline FH variants who might benefit from special genetic tests, and assessing tumor status preoperatively.

Based on an increasing interest in understanding the metabolic adaptations that occur during tumorigenesis (31) and how these adaptations might be exploited for novel therapeutic interventions, we have provided a method for clinical research that may be applied to assess the role of fumarate accumulation in

oncogenesis. Future studies could assess imaging markers correlated with fumarate levels with use of quantitative metrics, and in vivo research would be valuable for exploring the mechanism underlying fumarate accumulation and disease progression and treatment outcomes.

There were some limitations to our study. Point-resolved spectroscopy used in our study is the relatively low bandwidth of section-selective radiofrequency pulses, which results in chemical shift displacement and is affected by B_1 field inhomogeneity (32). Further studies should be carried out to optimize the experimental protocols using advanced MRS sequences (33) to increase the SNR of in vivo fumarate and improve the image quality. Moreover, considering that HLRCC is a rare disease and the number of participants enrolled is limited, further study with a larger sample is needed to ascertain the value of MRS in diagnosis of HLRCC-associated renal cancer in clinical work.

In conclusion, we demonstrated the application of MR spectroscopy (MRS) for the diagnosis of hereditary leiomyomatosis and renal cell carcinoma (HLRCC) syndrome–associated renal cancer. Abnormal fumarate accumulation was detected in vivo in both patient-derived xenograft models and participants, expanding the application of MRS to include primary HLRCC-associated renal cell carcinoma and related metastases.

Author contributions: Guarantors of integrity of entire study, **G.W., J.W., Y.X., J.Z.**; study concepts/study design or data acquisition or data analysis/interpretation, all authors; manuscript drafting or manuscript revision for important intellectual content, all authors; approval of final version of submitted manuscript, all authors; agrees to ensure any questions related to the work are appropriately resolved, all authors; literature research, **G.W., G.L., J.W., S.P., W.K., J.X., W.X., J.Z.**; clinical studies, **G.W., S.P., Y.L., Y.X., W.K., J.X., J.Z.**; experimental studies, **G.W., J.W., Y.L., J.X., W.X., J.Z.**; statistical analysis, **G.W., G.L., J.W., W.K., J.X.**; and manuscript editing, **G.W., G.L., J.W., W.K., P.S., J.X., J.Z.**

References

1. Tomlinson IP, Alam NA, Rowan AJ, et al. Germline mutations in FH predispose to dominantly inherited uterine fibroids, skin leiomyomata and papillary renal cell cancer. Nat Genet 2002;30(4):406–410.
2. Morin A, Letouzé E, Gimenez-Roqueplo AP, Favier J. Oncometabolites-driven tumorigenesis: from genetics to targeted therapy. Int J Cancer 2014;135(10):2237–2248.
3. Yang M, Soga T, Pollard PJ, Adam J. The emerging role of fumarate as an oncometabolite. Front Oncol 2012;2:85.
4. Menko FH, Maher ER, Schmidt LS, et al. Hereditary leiomyomatosis and renal cell cancer (HLRCC): renal cancer risk, surveillance and treatment. Fam Cancer 2014;13(4):637–644.
5. Grubb RL 3rd, Franks ME, Toro J, et al. Hereditary leiomyomatosis and renal cell cancer: a syndrome associated with an aggressive form of inherited renal cancer. J Urol 2007;177(6):2074–2079; discussion 2079–2080.
6. Choi Y, Keam B, Kim M, et al. Bevacizumab plus erlotinib combination therapy for advanced hereditary leiomyomatosis and renal cell carcinoma-associated renal cell carcinoma: a multicenter retrospective analysis in Korean patients. Cancer Res Treat 2019;51(4):1549–1556.
7. Chen YB, Brannon AR, Toubaji A, et al. Hereditary leiomyomatosis and renal cell carcinoma syndrome-associated renal cancer: recognition of the syndrome by pathologic features and the utility of detecting aberrant succination by immunohistochemistry. Am J Surg Pathol 2014;38(5):627–637.
8. Merino MJ, Torres-Cabala C, Pinto P, Linehan WM. The morphologic spectrum of kidney tumors in hereditary leiomyomatosis and renal cell carcinoma (HLRCC) syndrome. Am J Surg Pathol 2007;31(10):1578–1585.
9. Lehtonen HJ, Kiuru M, Ylisaukko-Oja SK, et al. Increased risk of cancer in patients with fumarate hydratase germline mutation. J Med Genet 2006;43(6):523–526.
10. Sun G, Zhang X, Liang J, et al. Integrated molecular characterization of fumarate hydratase-deficient renal cell carcinoma. Clin Cancer Res 2021;27(6):1734–1743.
11. Paschall AK, Nikpanah M, Farhadi F, et al. Hereditary leiomyomatosis and renal cell carcinoma (HLRCC) syndrome: spectrum of imaging findings. Clin Imaging 2020;68:14–19.
12. Northrup BE, Jokerst CE, Grubb RL 3rd, Menias CO, Khanna G, Siegel CL. Hereditary renal tumor syndromes: imaging findings and management strategies. AJR Am J Roentgenol 2012;199(6):1294–1304.
13. Choi C, Ganji SK, DeBerardinis RJ, et al. 2-hydroxyglutarate detection by magnetic resonance spectroscopy in IDH-mutated patients with gliomas. Nat Med 2012;18(4):624–629.
14. Casey RT, McLean MA, Madhu B, et al. Translating *in vivo* metabolomic analysis of succinate dehydrogenase deficient tumours into clinical utility. JCO Precis Oncol 2018;2:1–12.
15. Tiwari V, Daoud EV, Hatanpaa KJ, et al. Glycine by MR spectroscopy is an imaging biomarker of glioma aggressiveness. Neuro Oncol 2020;22(7):1018–1029.
16. Casey RT, McLean MA, Challis BG, et al. Fumarate metabolic signature for the detection of Reed syndrome in humans. Clin Cancer Res 2020;26(2):391–396.
17. Huang SY, Seethamraju RT, Patel P, Hahn PF, Kirsch JE, Guimaraes AR. Body MR imaging: artifacts, k-space, and solutions. RadioGraphics 2015;35(5):1439–1460. [Published correction appears in RadioGraphics 2015;35(5):1624.]
18. Patel VM, Handler MZ, Schwartz RA, Lambert WC. Hereditary leiomyomatosis and renal cell cancer syndrome: an update and review. J Am Acad Dermatol 2017;77(1):149–158.
19. Agarwal M, Chawla S, Husain N, Jaggi RS, Husain M, Gupta RK. Higher succinate than acetate levels differentiate cerebral degenerating cysticerci from anaerobic abscesses on in-vivo proton MR spectroscopy. Neuroradiology 2004;46(3):211–215.
20. Bartella L, Morris EA, Dershaw DD, et al. Proton MR spectroscopy with choline peak as malignancy marker improves positive predictive value for breast cancer diagnosis: preliminary study. Radiology 2006;239(3):686–692.
21. Martin P, Bateson P. Measuring Behaviour: An Introductory Guide. 3rd ed. Cambridge, UK: Cambridge University Press, 2007.
22. Lau HD, Chan E, Fan AC, et al. A clinicopathologic and molecular analysis of fumarate hydratase-deficient renal cell carcinoma in 32 patients. Am J Surg Pathol 2020;44(1):98–110.
23. Gupta S, Swanson AA, Chen YB, et al. Incidence of succinate dehydrogenase and fumarate hydratase-deficient renal cell carcinoma based on immunohistochemical screening with SDHA/SDHB and FH/2SC. Hum Pathol 2019;91:114–122.
24. Bardella C, El-Bahrawy M, Frizzell N, et al. Aberrant succination of proteins in fumarate hydratase-deficient mice and HLRCC patients is a robust biomarker of mutation status. J Pathol 2011;225(1):4–11.
25. Buelow B, Cohen J, Nagymanyoki Z, et al. Immunohistochemistry for 2-succinocysteine (2SC) and fumarate hydratase (FH) in cutaneous leiomyomas may aid in identification of patients with HLRCC (hereditary leiomyomatosis and renal cell carcinoma syndrome). Am J Surg Pathol 2016;40(7):982–988.
26. Egbert ND, Caoili EM, Cohan RH, et al. Differentiation of papillary renal cell carcinoma subtypes on CT and MRI. AJR Am J Roentgenol 2013;201(2):347–355.
27. Fu W, Huang G, Moloo Z, Girgis S, Patel VH, Low G. Multimodality imaging characteristics of the common renal cell carcinoma subtypes: an analysis of 544 pathologically proven tumors. J Clin Imaging Sci 2016;6:50.
28. Ching BC, Tan HS, Tan PH, et al. Differential radiologic characteristics of renal tumours on multiphasic computed tomography. Singapore Med J 2017;58(5):262–266.
29. Yamada T, Endo M, Tsuboi M, et al. Differentiation of pathologic subtypes of papillary renal cell carcinoma on CT. AJR Am J Roentgenol 2008;191(5):1559–1563.
30. Xu L, Gu S, Feng Q, Liang C, Xin SX. Quantitative study of liver magnetic resonance spectroscopy quality at 3T using body and phased array coils with physical analysis and clinical evaluation. PLoS One 2015;10(4):e0122999.
31. Keunen O, Niclou SP. Is there a prominent role for MR spectroscopy in the clinical management of brain tumors? Neuro Oncol 2020;22(7):903–904.
32. Andronesi OC, Rapalino O, Gerstner E, et al. Detection of oncogenic IDH1 mutations using magnetic resonance spectroscopy of 2-hydroxyglutarate. J Clin Invest 2013;123(9):3659–3663.
33. Garwood M, DelaBarre L. The return of the frequency sweep: designing adiabatic pulses for contemporary NMR. J Magn Reson 2001;153(2):155–177.